A resonance enhanced multiphoton ionization study of the gerade excited states of XeC2 with a Xe E1SC0 + XeE* 6s[3/2]C1 dissociation limit

Koeckhoven, S.M.; Buma, W.J.; de Lange, C.A.

DOI
10.1063/1.468530
Publication date
1995

Published in
Journal of Chemical Physics

A resonance enhanced multiphoton ionization study of the gerade excited states of Xe_2 with a $Xe\ ^1S_0+Xe^*\ 6s[3/2]_1$ dissociation limit

S. M. Koeckhoven, W. J. Buma, and C. A. de Lange
Laboratory for Physical Chemistry, University of Amsterdam, Nieuwe Achtergracht 127, 1018 WS Amsterdam, The Netherlands

(Received 3 October 1994; accepted 30 November 1994)

Low-lying *gerade* electronically excited states of the Xe dimer, viz., 1_g and 0_g^+, with a $Xe\ ^1S_0+Xe^*\ 6s[3/2]_1$ dissociation limit have been investigated using two-photon resonance enhanced multiphoton ionization techniques. High resolution is achieved by using this method in combination with a supersonic expansion. Moreover, the mass-resolved ion detection used in the present experiments has led to the observation of both vibrationally well-resolved spectra and continuous features, allowing the bound and dissociative parts of the excited states to be investigated separately. All spectra have been measured under both linearly and circularly polarized excitation conditions, enabling an unambiguous assignment of the signals. On the basis of Franck–Condon calculations information on the potential energy curves of the bound and dissociative parts of the excited states has been obtained. © *1995 American Institute of Physics.*

I. INTRODUCTION

The study of weakly bound complexes involving rare gas atoms is interesting for both fundamental and practical reasons. First, transition states which play a key role in chemical reactions often show bonding characteristics similar to those found in such complexes.[1] Secondly, detailed knowledge about excited states of van der Waals complexes containing rare gas atoms is helpful in understanding the chemical mechanisms occurring in a large variety of excimer lasers.[2,3]

A prototype example of a van der Waals complex is the Xe dimer. In the ground state of the dimer all valence orbitals deriving from $5p$ atomic orbitals are occupied. The potential energy curve is mainly dissociative with a shallow minimum at large internuclear distances. Excitation of a valence electron leads to states which may have bonding characteristics very different from that of the ground state. In fact, both bound and fully dissociative states can be addressed in this fashion.[4–16]

The study of excited states of van der Waals complexes is no trivial matter. Due to experimental difficulties in producing these complexes under isolated conditions, and in view of the generally rather poor Franck–Condon overlap between the weakly bound ground state and the excited states, detailed information about potential energy curves of these species has mostly become available during the last decade. A useful way of accessing excited states of van der Waals complexes is through one-photon absorption from the ground state. In view of the gerade character of the Xe_2 ground state such studies have produced ample information about its *ungerade* excited states.[4,6,9,12,14,16] Gerade excited states, which can only be reached in a two-photon process[5,7,8,10,11,13,15] involving high-intensity lasers, have received considerably less attention.

Studies of *gerade* excited states of Xe_2 have been mainly restricted to Rydberg states with $Xe\ ^1S_0+Xe^*(5d\leftarrow\leftarrow 5p)$ and $Xe\ ^1S_0+Xe^*\ (6p\leftarrow\leftarrow 5p)$ dissociation limits.[5,10,11,13,15] For many of these states potential energy curves have been studied in some detail. In contrast, information on *gerade* excited states with a $Xe\ ^1S_0+Xe^*\ (6s\leftarrow\leftarrow 5p)$ dissociation limit is still scanty.[7,8]

The two *gerade* excited states occurring in the energy region near the $Xe\ ^1S_0+Xe^*\ 6s[3/2]_1$ dissociation limit, viz., 1_g and 0_g^+, have been addressed in previous experimental studies.[7,8] These experiments have been carried out in a gas cell at ambient temperature with fluorescence detection. As a result, broad rotational structures and hot bands could not be avoided, leading to unresolved features in the excitation spectra for both electronic states. This difficulty was augmented by the use of fluorescence as a detection technique, because the fluorescence signal does not only depend on the excitation process, but also on the relaxation mechanisms. Since gerade states cannot fluoresce directly to the *gerade* ground state, the excitation spectra are expected to be strongly influenced by these relaxation processes. No information on the potential energy curves could be derived from these experiments.

In the present work the same 1_g and 0_g^+ excited states with a $Xe\ ^1S_0+Xe^*\ 6s[3/2]_1$ dissociation limit are studied employing different experimental techniques by which the above problems could be circumvented. The measurements in the present study are performed under ideal conditions of complex isolation and low temperature which prevail in a pulsed supersonic expansion. High spectral resolution is obtained by combining this molecular beam method with two-photon resonance enhanced multiphoton ionization (REMPI). The dependence of the signal intensities on the polarization of the excitation light is used for unambiguous assignments of the spectra. In addition, the use of mass-resolved ion detection allows for the separate investigation of the bound and repulsive parts of the 1_g and 0_g^+ potential energy curves, leading to new information about these potentials.

II. EXPERIMENT

The experimental setup is similar to the one used in previous multiphoton ionization studies,[17] and therefore only a

 0021-9606/95/102(10)/4020/7/$6.00

summary will be given. The laser system consists of an excimer pumped dye laser (bandwidth 0.08 cm^{-1}) which operated on the dye rhodamine 6G. The output of the dye laser is frequency-doubled in an autotracking unit equipped with a KDP crystal. The polarization of the frequency-doubled light, which is initially linear with a purity of 1000:1, can be modified continuously with a Pockels cell. Circularly polarized light can in this way be generated with a purity of 300:1.

For the alignment and adjustment of the Pockels cell the $8s'[1/2]_1$ autoionizing resonance of atomic Xe was used, which can be reached by a three-photon absorption from the ground state.[18] The one-photon energy for this transition is close to the one-photon energies used in the present study and its signal intensity strongly depends on the polarization of the excitation light. For absolute wavelength calibration the well-known optogalvanic spectrum of Ne,[19] excited in a hollow-cathode lamp, was used. In this way the fundamental wavelength could be determined with an accuracy of 0.3 cm^{-1}.

The laser beam is focused into a supersonic expansion generated by a General Valve Iota One System. Ions produced in the multiphoton ionization process are focused into the entrance of a quadrupole mass spectrometer, whose mass resolution can be adjusted. Adjustment of the resolution, however, also influences the ion transmission of the filter. Since the ion signals in the present study were very small, the filter was optimized for the transmission, which consequently resulted in a lower mass resolution. The different isotopes of Xe and Xe_2 were therefore not resolved. Atomic and dimer ions, however, were easily separated. Ions of Xe_n with $n \geqslant 3$ could not be detected, since their masses are outside the mass range of the quadrupole filter.

The excitation spectra appear to be strongly dependent on the expansion conditions. Changing these conditions resulted in either large background signals, which are attributed to larger clusters, or in a strong decrease of the dimer signal. The experimental parameters such as size of the pinhole, distance between the point of ionization and the nozzle, backing pressure, gas pulse duration, and timing of the laser pulse were carefully optimized in order to create an expansion with maximum dimer concentration and few larger clusters. Spectra shown in the present study are measured with a pinhole of 100 μm. Backing pressures of 0.5 bar for a pure Xe expansion or of 3 bar for an expansion of 5% Xe seeded in He were used. Ionization was performed at a distance of more than 10 mm from the nozzle. The results to be described below indicate that under such expansion conditions a rotational cooling down to 3 K is achieved.

III. RESULTS

In Fig. 1 the (2+1) REMPI spectrum of the 1_g electronic state of Xe_2 with a Xe $^1S_0$+Xe* $6s[3/2]_1$ dissociation limit is presented. The spectrum, obtained by detecting dimer ions, shows a progression of about 25 discrete vibrational resonances. The progression starts at the low-energy side with small well-resolved transitions, which are slightly degraded to the red. Using an expansion of either pure Xe or a mixture of 5% Xe seeded in He resulted in slightly different line shapes of the resonances. The signal intensities of the resonances increase monotonically with vibrational quantum number, reaching a maximum, and then decrease again. The spacing between the resonances decreases with vibrational quantum number, leading to overlapping resonances and finally to a nonresolved structure. At the high energy side of the spectrum the signal drops sharply and vanishes completely at a one-photon energy of 34 114.8 cm^{-1}.

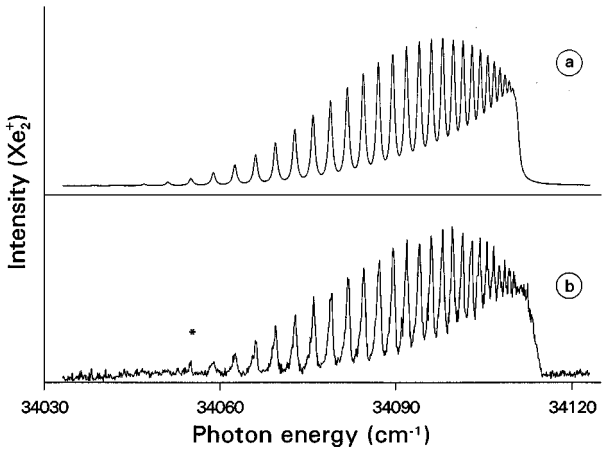

FIG. 1. High resolution (2+1) REMPI spectrum of Xe_2 in the energy region near the Xe $^1S_0$+Xe* $6s[3/2]_1$ dissociation limit. (a) Simulated spectrum based on a Morse potential energy curve derived from the experimental spectrum using a $v'=5$ assignment for the first observed vibrational level (marked with an asterisk). (b) Experimental spectrum.

In Fig. 2(a) an excitation spectrum is presented which is obtained by detecting atomic ions. The atomic ions can be created via different mechanisms, the most likely of which will be discussed. First, atomic ions can be created by nonresonant three-photon ionization of nonclustered Xe atoms, which are abundantly present in the supersonic expansion. Secondly, they can arise from dissociation processes in the Xe dimer ion. For such a process to occur the Xe dimer has to be excited at least above the lowest dissociation limit of the dimer ion, which under the present experimental conditions can be achieved by the absorption of only three photons. Finally, they can be created in a direct photodissociation process. In such a process the dimer is excited by a two-photon absorption to a dissociative part of an electronically excited state and dissociates into a Xe atom in its ground state and a Xe atom in an excited state. The electronically excited fragment is subsequently ionized by the absorption of an additional photon, thus creating the Xe^+ ions.

The two-photon energy in Fig. 2(a) is scanned from about 200 cm^{-1} below to about 1000 cm^{-1} above the Xe $^1S_0$+Xe* $6s[3/2]_1$ dissociation limit of the Xe dimer. The spectrum shows two broad features superimposed on a small background continuum. The two broad features are attributed to the 1_g and 0_g^+ electronic states of Xe_2 with a Xe $^1S_0$+Xe* $6s[3/2]_1$ dissociation limit, while the continuum is attributed to nonresonant ionization of Xe atoms.

The broad feature assigned to the 1_g electronic state has intensity below as well as above the Xe $^1S_0$+Xe* $6s[3/2]_1$ dissociation limit. The structure below the limit shows much resemblance to the (2+1) REMPI spectrum of Xe_2 given in Fig. 1(b). These atomic signals therefore originate via a

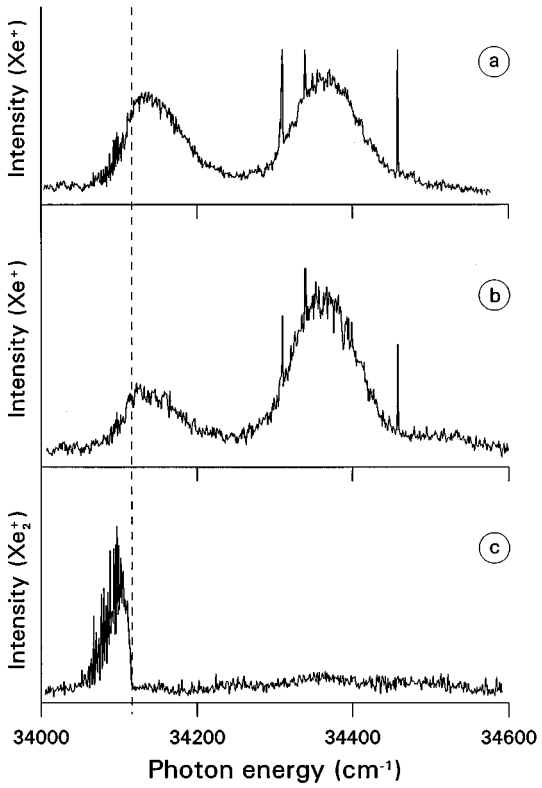

FIG. 2. Low resolution REMPI spectra of Xe_2 in the energy region near the $Xe\ ^1S_0+Xe^*\ 6s[3/2]_1$ dissociation limit. The dashed line shown in the figure gives the energy position of this limit. (a) Two-photon excitation spectrum of Xe_2 by detecting atomic Xe^+ ions, using circularly polarized excitation light. (b) Two-photon excitation spectrum of Xe_2 by detecting atomic Xe^+ ions, using linearly polarized excitation light. (c) Two-photon excitation spectrum of Xe_2 by detecting molecular Xe_2^+ ions, using linearly polarized excitation light.

mechanism which starts with a two-photon transition in the dimer to bound vibrational levels associated with the 1_g electronic state. Atomic ions are subsequently formed by dissociation of the dimer ion. The signal above the dissociation limit is structureless and has an almost Gaussian line shape [FWHM (one-photon energy)$=112\ cm^{-1}$]. These Xe^+ signals may arise from excitation of the dimer to dissociative parts of the 1_g electronic state and subsequent ionization of excited atomic fragments.

The second broad structureless feature, attributed to the 0_g^+ electronic state, has also an almost Gaussian line shape [FWHM (one-photon energy)$=99\ cm^{-1}$]. This atomic signal similarly arises via excitation to the dissociative part of the electronically excited state followed by dissociation and ionization processes. Our experimental results show no evidence for any bound character of this 0_g^+ electronic state.

Superimposed on the 0_g^+ structureless feature three narrow resonances are observed. These atomic signals have not been identified, but they probably arise from electronically excited atoms formed in dissociation processes. Since these signals are not thought to be associated with the 1_g and 0_g^+ electronic states of the Xe dimer, no further attention will be given to them.

The spectrum shown in Fig. 2(a) was measured under circularly polarized excitation conditions. By changing the polarization of the excitation light to linear, the spectrum depicted in Fig. 2(b) is observed. The shapes of the two broad features are identical under both polarization conditions. The intensities, however, depend on the polarization of the light. The signal attributed to the 1_g electronic state decreases as the polarization is changed from circular to linear: $S_{cir}/S_{lin}\ (1_g)=1.51(0.2)$. Here S_{cir} and S_{lin} are defined as the signal intensity measured with circularly and linearly polarized excitation light, respectively. The 0_g^+ state shows a different dependency on the polarization $[S_{cir}/S_{lin}\ (0_g^+)=0.62(0.1)]$. The observation that the two broad features exhibit a different polarization dependence unambiguously shows that they derive from excitation of two different electronic states.

In Fig. 2(c) the (2+1) REMPI spectrum of the 1_g electronic state of Xe_2 is presented in the same energy range as Figs. 2(a) and 2(b). Note that this spectrum was obtained by detecting dimer ions, whereas in the spectra shown in Figs. 2(a) and 2(b) atomic ions were detected. By detecting atomic ions signal is observed below as well as above the $Xe\ ^1S_0+Xe^*\ 6s[3/2]_1$ dissociation limit. In contrast, when dimer ions are monitored, signal is only observed below the dissociation limit. The spectrum in Fig. 2(c) shows that excitation to dissociative parts of the 1_g and 0_g^+ electronic states is not followed to a significant extent by ionization of the dimer. Apparently, under the present experimental conditions, the dissociation process is much faster than the ionization process.

IV. DISCUSSION

A. 1_g electronic state: Discrete spectrum

The experimental spectrum of the 1_g electronic state presented in Fig. 1 shows a long vibrational progression. This generally indicates that the potential energy curve of the excited state has an equilibrium distance markedly different from that of the ground state. Since the intensities of the resonances decrease smoothly and finally vanish completely in going to lower vibrational levels, the first observed resonance cannot automatically be assigned to $v'=0$. Isotope splittings in such cases can be a useful tool for the determination of an absolute quantum numbering.[15] Since isotope splittings are not resolved in the present experiments an alternative approach based on energy positions and intensities of the resonances was adopted.

For the description of the potential energy curve of the 1_g excited state a simple Morse curve was assumed. The shape of this potential is defined by the constants ω_e and $\omega_e\chi_e$, while its position is determined by T_e and R_e.[20] The anharmonicity constant $\omega_e\chi_e$ of the excited state potential can be obtained from our experimental results using a Birge–Sponer plot,[20] since for such an analysis an absolute vibrational quantum numbering is not necessary. For any chosen absolute vibrational numbering the constants ω_e and T_e can be derived from the energy positions of the vibrational components. This choice therefore completely determines the *shape* of the Morse potential. The remaining parameter re-

TABLE I. Molecular constants for the 1_g state with a $Xe\ ^1S_0+Xe^*\ 6s[3/2]_1$ dissociation limit using Morse potentials obtained by least-square fits to both energy positions and intensities of the vibrational resonances of the discrete spectrum.

Assignment to lowest observed resonance	Resonances used in spectral analysis	T_e (cm^{-1})	ω_e (cm^{-1})	$\omega_e\chi_e$ (cm^{-1})	R_e (bohr)
$v'=5$	all	68 073.8(3)	9.21(0.4)	0.134(0.01)	10.19(0.08)
$v'=4$	first 12	68 082.0(1.5)	9.10(0.3)	0.140(0.01)	10.12(0.08)

quired to fix the *position* of the Morse curve is the location of its minimum at internuclear distance R_e.

For any given vibrational numbering the value of R_e can be optimized by considering the Franck–Condon factors between the lowest vibrational level associated with the ground state of the dimer and the vibrational levels of the 1_g excited state. The $v''=0$ vibrational wave function of the ground state is calculated analytically using known Morse parameters.[21,22] The vibrational wave functions associated with the 1_g state can be calculated if a value of R_e is assumed. The relevant Franck–Condon factors can now be computed numerically, and by introducing Gaussian and/or Lorentzian line shapes the experimental spectrum can be simulated. The value of R_e is adjusted until the best least-squares agreement between experimental and calculated spectra is achieved.

Two calculations have been performed. In the first calculation all observed resonances are employed in the least-squares fit, leading to an assignment of the first vibrational feature (marked with an asterisk in Fig. 1) as $v'=5$ and the Morse potential parameters given in Table I. The calculated spectrum using this Morse potential energy curve is shown in Fig. 1(a). In the second calculation, on the other hand, only the first 12 observed resonances are fitted. Excellent agreement between experimental and theoretical Franck–Condon factors is now obtained when the first vibrational component is assigned to $v'=4$. The Morse curve and its associated parameters are given in Fig. 3 and Table I, respectively.

The results of these two calculations indicate that the description of the 1_g potential with a Morse curve is reasonably good for intermediate distances, but shows some inadequacies at both small and large internuclear distances. In the first calculation, in which effectively the complete range of accessible internuclear distances is of importance, these inadequacies lead to a nonrandom distribution of the residuals of the energy levels, a faster drop of the intensity at the high-energy side of the calculated spectrum than in the experimental spectrum, and a significant difference between the dissociation limit of the Morse potential (68 221.8 cm^{-1}) (Ref. 21) and the limit determined from the experimental spectrum (68 229.6 cm^{-1}). The fact that a simple Morse potential does not exactly describe the potential curve of the 1_g electronic state manifests itself in the second calculation, where only intermediate internuclear distances are probed, in the simulation of the complete spectrum using the parameters determined from this fit. Here, the simulated Franck–Condon factors of higher vibrational levels are underestimated indicating that the repulsive part of the real potential at small internuclear distances is steeper than that described by the Morse curve. Despite the fact that the true potential is not known in every detail, a $v'=4\pm2$ assignment of the lowest observed vibrational component would appear reasonable.

In the analysis of the experimental spectrum the position and integrated intensities of the vibrational resonances have been used. The widths and line shapes of these resonances contain, however, also information on the excited state. Analysis of the experimental spectrum shows that the widths are almost identical for all observed vibrational components and that the resonances are slightly degraded to the red. In principle the widths and line shapes depend on both isotope

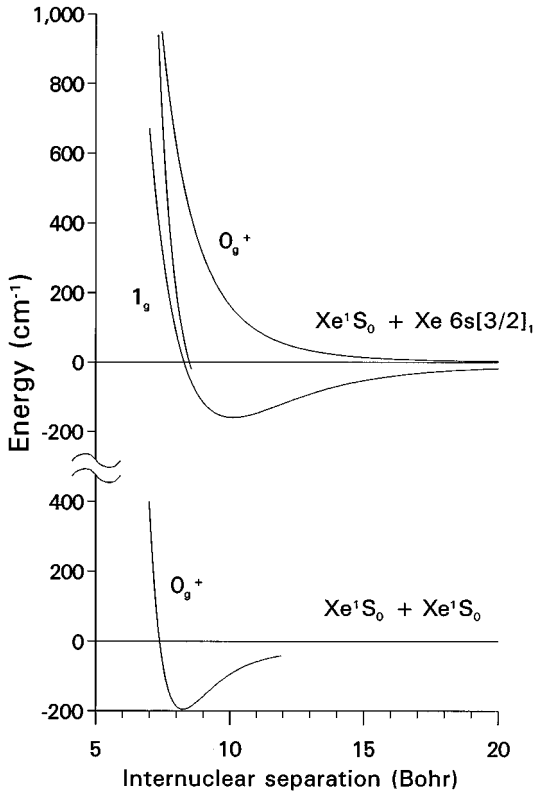

FIG. 3. Potential energy curves of the ground state (Ref. 21) and the 1_g and 0_g^+ excited states with a $Xe\ ^1S_0+Xe^*\ 6s[3/2]_1$ dissociation limit obtained in the present study. For the 1_g state the Morse potential energy curve derived from the discrete spectrum using a $v'=4$ assignment for the lowest observed resonance is shown. The parameters for this curve are given in Table I. In addition, a curve which describes the potential of the 1_g state at small internuclear distances above the dissociation limit is given. This curve is derived from the continuous spectrum of the 1_g state. For the 0_g^+ state a fully dissociative potential energy curve is shown. The energy scale on the y-axis is relative to the dissociation limits of the electronic states.

effects and rotational structures. The calculated broadening due to unresolved isotope structure ($\leqslant 0.5$ cm^{-1}) is considerably smaller than the experimentally observed width (FWHM$=1.5$ cm^{-1}), indicating that the resonances are predominantly affected by rotational structure. This is also confirmed by the fact that the shapes and widths were found to be dependent on the expansion conditions, which in effect determine the rotational temperature. Moreover, the observed red-degraded line shapes can be simulated quite well assuming a ($^1\Pi \leftarrow\leftarrow {}^1\Sigma^+$) transition (vide infra) and using the rotational constant estimated from the potential energy curve based on the $v'=4$ assignment. The rotational structures therefore confirm the earlier notion that the equilibrium distance of the molecule in the excited state is larger than that in the ground state.

B. 1_g and 0_g^+ electronic states: Continuous spectra

The spectra in which atomic ions are detected [Figs. 2(a) and 2(b)] derive from the dissociative parts of the dimer potential energy curves. These curves of the 1_g and 0_g^+ electronic states above the Xe $^1S_0$+Xe* $6s[3/2]_1$ dissociation limit are determined using Franck–Condon analyses. In these analyses the Franck–Condon factors between the ground state $v''=0$ vibrational wave function and the continuum vibrational wave functions of the excited states are calculated. The vibrational wave functions of the excited states are obtained at energies starting just above the dissociation limit to a thousand wave numbers above it. The ground state wave functions are again analytically calculated using known Morse parameters,[21,22] the continuum vibrational wave functions of the excited states are calculated using a numerical integration scheme based on the Numerov method.[23] In the analyses of the excitation spectra it is assumed that the atomic signal is proportional to the Franck–Condon factors between the ground and excited state vibrational wave functions of the dimer.

Using the Morse potential curve for the 1_g electronic state determined from the discrete part of the spectrum to simulate the continuum part a rather large disagreement with the experimental spectrum is found. This disagreement is expected since, as has already been concluded from the discrete spectrum, the repulsive part of the Morse potential at small internuclear distances is not steep enough. Therefore, a simple Ar^{-12}–B potential, in which the parameters A and B serve to mimic the repulsive part of the real potential, is used. Excellent agreement is found for $A=2.72\times10^{13}$ cm^{-1} Bohr^{12} and $B=195$ cm^{-1}, as can be seen in Fig. 4. The curve, which is shown in Fig. 3, gives an indication of the position and steepness of the real potential energy curve just above the dissociation limit.

For the 0_g^+ electronic state with a Xe $^1S_0$+Xe* $6s[3/2]_1$ dissociation limit no evidence of bound character is found. The spectrum, therefore, is analyzed using a very simple analytical function which is completely dissociative (Ar^{-n}) and which for large internuclear distances approaches the correct dissociation limit. Very good agreement between simulated and experimental spectra is found for $n=6$ and $A=1.63\times10^8$ cm^{-1} Bohr^6 as is shown in Fig. 4.

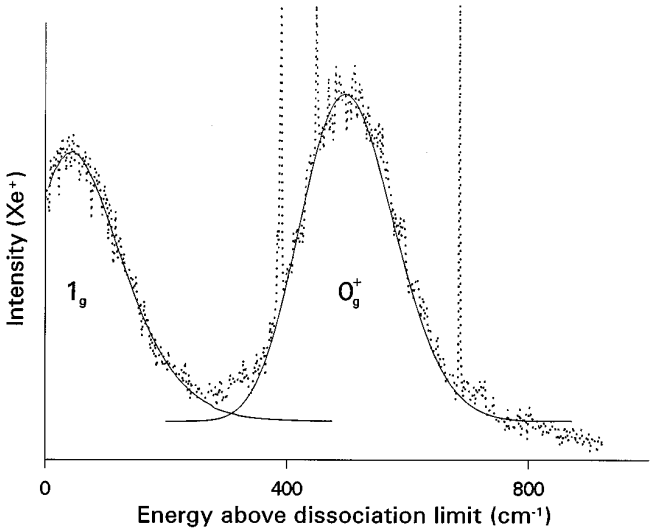

FIG. 4. Two-photon excitation spectrum of Xe_2 by detecting atomic Xe^+ ions above the Xe $^1S_0$+Xe* $6s[3/2]_1$ dissociation limit. The experimental continuous spectrum (···) is given together with the simulated continuous spectra (—) of both the 1_g and 0_g^+ states. The energy scale on the x axis is relative to the dissociation limit.

In summary, the potential energy curves above the dissociation limit of the 1_g and 0_g^+ electronic states can be described quite well by simple analytical functions. It has to be kept in mind, however, that these potentials are established for internuclear distances at which there is Franck–Condon overlap with the $v''=0$ ground state wave function. The real potentials outside this Franck–Condon region may well show deviations from this behavior.

C. Assignments

In a simple one-electron picture excited states of the Xe dimer can be described by an ionic core with a Rydberg electron. States with Xe $^1S_0$+Xe* $(6s,6s')$ dissociation limits, which are of interest in the present study, form the lowest members of Rydberg series converging to the six lowest ionic states with Xe $^1S_0$+Xe^+ ($^2P_{3/2}$,$^2P_{1/2}$) dissociation limits. The Rydberg electron of these molecular excited states is of $6s\sigma_g$ symmetry.[24,25] In Fig. 5 a diagram is presented in which molecular states derived from dimer electronic configurations are correlated to molecular states derived from the appropriate dissociation limits. The electron configurations considered in the diagram involve excitation of a $5p\sigma_u$, $5p\pi_g$, $5p\pi_u$, or $5p\sigma_g$ valence electron to the lowest unoccupied molecular $6s\sigma_g$ orbital. Dissociation limits with one atom in the ground state and one atom with a $5p$ electron excited to the lowest unoccupied atomic orbital ($6s$) are included.

On the left-hand side in the diagram molecular states are given using Hund's case (a) notation [$^{2S+1}\Lambda(\Omega_{g/u})$]. The ordering of these excited states as well as that of the ionic states has been drawn schematically for an internuclear distance which is equal to the equilibrium distance of the ground state and has been obtained from the study of Ermler *et al.*[25] On the right-hand side the molecular states are con-

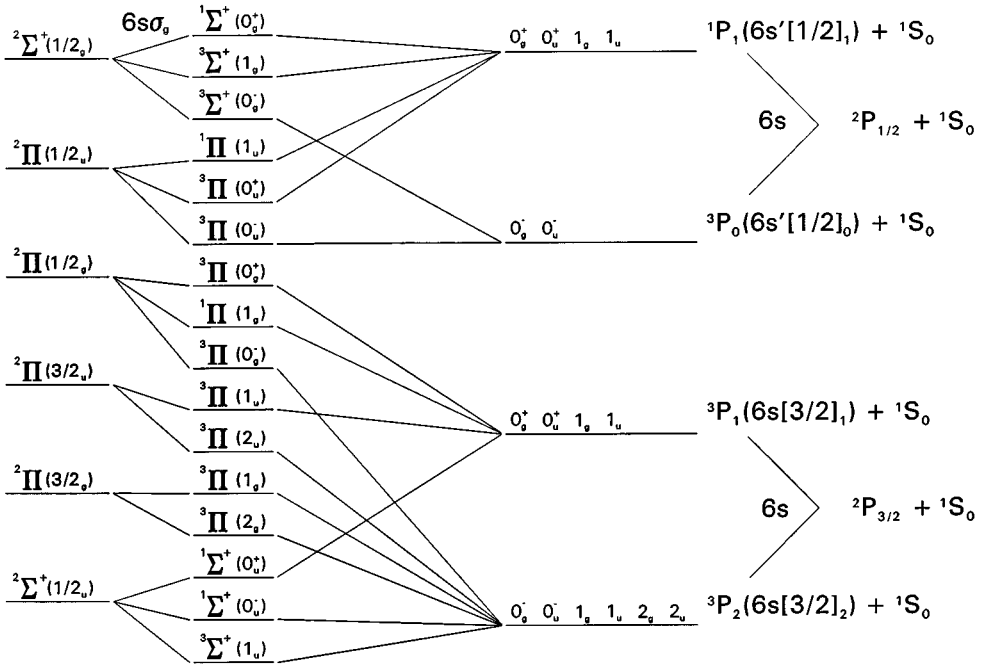

FIG. 5. Correlation diagram between molecular dimer states at a distance corresponding to the equilibrium distance in the ground state and in the separated atom approximation (see text for explanation).

sidered in the separated atom limit. Here, the atomic states are given using both LS coupling ($^{2S+1}L_J$) and $j_c l$ coupling $[nl'(j_{\text{core}}+l_{\text{Rydberg electron}})_J]$ notation.[26]

In the Xe dimer only Ω, the projection of the total electronic angular momentum on the internuclear axis, rather than Λ and Σ separately, is a well-defined quantum number.[24,25,27] In the diagram electronic states derived from electron configurations and dissociation limits are therefore adiabatically correlated using only $\Omega_{g/u}$. The diagram might seem to suggest that the excited states of the Xe dimer can be described by a single electron configuration. Such a description will in general not be valid since states with identical values of $\Omega_{g/u}$ can mix. Moreover, it should be stressed that in the correlation diagram only electron configurations with a $6s\sigma_g$ Rydberg electrons are considered. This description is appropriate at large internuclear distances, but at smaller internuclear distances electron configurations with other Rydberg electrons will also become important.[24]

For the assignments of the signals observed in the present study selection rules, polarization dependence of the signal intensities, and dissociation limit considerations will be used. According to two-photon absorption selection rules in Hund's case (c), only states with $\Omega_{g/u}=2_g$, 1_g, and 0_g^+ can be excited from the 0_g^+ ground state.[28] Since the ground state of the Xe dimer is mainly described by the $^1\Sigma^+(0_g^+)$ wave function, the transition to the 2_g state, which has only spin triplet character,[7] is spin-forbidden. The signals observed in the present study must consequently arise from 1_g and/or 0_g^+ electronic states.

The intensities of the signals were measured as a function of the polarization of the excitation light. For the bound state a ratio $S_{\text{cir}}/S_{\text{lin}}=1.51(0.2)$ was obtained, while for the completely dissociative state this ratio was found to be 0.62(0.1). The observation of different polarization dependencies directly indicates that two different kinds of transitions are involved. The transitions to the 1_g and 0_g^+ states obtain their intensities from their $^1\Pi(1_g)$ and $^1\Sigma^+(0_g^+)$ spin singlet characters, respectively.[7] Theoretically, the polarization dependencies of these transitions are predicted as[29] $S_{\text{cir}}/S_{\text{lin}}$ ($^1\Pi\leftarrow\leftarrow{}^1\Sigma$)=1.5 and $S_{\text{cir}}/S_{\text{lin}}$ ($^1\Sigma\leftarrow\leftarrow{}^1\Sigma$)$\leqslant$1.5. The dissociative state can therefore be assigned as a 0_g^+ state. Consequently, the bound state has to be a 1_g state.

We thus have now established the quantum numbers of the excited states; Ω_g(bound state)$=1_g$ and Ω_g(dissociative state)$=0_g^+$. It now remains to choose the correct dissociation limits. For the bound state the dissociation limit determined from the experimental spectrum is 68 229.6 cm^{-1}. This value agrees perfectly with the limit determined from the dissociation energy D_0'' of the dimer ground state[21] and the excitation energy of the $6s[3/2]_1$ atomic excited state[26] (68 231.7 cm^{-1}). It can therefore be concluded that the bound 1_g excited state has a Xe $^1S_0$+Xe* $6s[3/2]_1$ dissociation limit. For the completely dissociative state a continuous spectrum is observed for two-photon energies between 68 500 and 69 000 cm^{-1}. Since the dissociation limit of this electronic state must be lower in energy, its limit is either Xe $^1S_0$+Xe* $6s[3/2]_1$ or Xe $^1S_0$+Xe* $6s[3/2]_2$. The combination of Xe $^1S_0$+Xe* $6s[3/2]_2$ does not result in a 0_g^+ state. Consequently, the dissociation limit of the completely dissociative 0_g^+ state has to be Xe $^1S_0$+Xe* $6s[3/2]_1$.

One might be tempted to try to assign the bound 1_g and dissociative 0_g^+ states as Rydberg states with one particular ionic core, i.e., use a single-electron configuration to describe these states. As mentioned above, the validity of such a description will be determined to a large extent by the

mixing of states with the same values of $\Omega_{g/u}$. Nevertheless, in first approximation, in which such mixing is assumed to be small, the diagram in Fig. 5 suggests that the bound 1_g state has predominantly $^1\Pi(1_g)$ character, while the dissociative 0_g^+ state is correlated with the $^3\Pi(0_g^+)$ state. Within the single-electron configuration picture both states would consequently have a $^2\Pi(1/2_g)$ ionic core. The potential energy curve of this ionic state has recently been calculated.[27] The predicted potential is mainly dissociative apart from a shallow well with a depth of 78 cm^{-1} at an internuclear distance $R_e=12$ bohr. The potentials of the 1_g and 0_g^+ states determined in the present study are different from this potential.

When we assume less stringent conditions on the description of the 1_g and 0_g^+ states by allowing for configuration mixing within the $6s\sigma_g$ complex, the diagram shows that also configurations with a $^2\Sigma(1/2_g)$ ionic core can be of importance. For this state calculations predict a potential with a dissociation energy of 242 cm^{-1} and an equilibrium distance of 10.0 bohr.[27] As far as the bound 1_g state is concerned, these numbers would seem to suggest a better agreement with a description in terms of a $^2\Sigma(1/2_g)$ ionic core. More information about the description of the two states might be obtained with photoelectron spectroscopy.

The potential energy curves of the 1_g and 0_g^+ states have been investigated in a few theoretical studies.[24,25] At large internuclear distances the results from those studies were in qualitative agreement. For the 1_g state some bound character was predicted with a minimum in the potential at about 8 bohr, whereas for the 0_g^+ state a fully dissociative potential was obtained as long as the state is described as an ion core with a $6s\sigma_g$ Rydberg electron. The results of these calculations agree reasonably well with those of the present study. A more detailed comparison, however, reveals that the bound region of the 1_g potential is not described completely correctly by theory and that the theoretical potentials are shifted to slightly smaller internuclear distances.

V. CONCLUSIONS

The present study shows that electronically excited states of weakly bound species can be studied in detail using REMPI combined with mass-resolved ion detection. High resolution was achieved by using narrow band laser light and ideal experimental conditions created in a supersonic expansion enabling the observation of vibrationally well-resolved excitation spectra of the Xe dimer.

In the present study two gerade electronically excited states, viz., 1_g and 0_g^+, with a $Xe\ ^1S_0+Xe^*\ 6s[3/2]_1$ dissociation limit have been studied. The excitation spectra have been measured under both linearly and circularly polarized excitation conditions. Using the dependence of the signal intensities on the polarization of the light, an unambiguous assignment of the signals observed in the present experiment could be given. By using mass-resolved ion detection the bound and dissociative parts of the potential energy curves could be investigated separately. Vibrational structure was only observed for the 1_g state. Transitions from the ground state to dissociative parts of the potential energy curves were detected for both electronic states. On the basis of Franck–Condon calculations information on both the bound (1_g) and dissociative $(1_g,0_g^+)$ parts of the potential energy curves have been obtained. From our experiments we conclude that the 1_g electronic state is a bound state, whereas our spectra show no evidence for any bound character for the 0_g^+ state.

ACKNOWLEDGMENTS

We gratefully acknowledge B. Rooswijk and Ing. D. Bebelaar for their technical skills, and the Netherlands Organization for Scientific Research (N.W.O.) for equipment grants and financial support.

[1] J. A. Beswick and J. Jortner, Adv. Chem. Phys. **47**, 363 (1981).
[2] M. Krauss and F. H. Mies, *Excimer Lasers*, edited by Ch. K. Rhodes (Springer, Berlin, 1984).
[3] J. Xu and D. W. Setser, J. Chem. Phys. **92**, 4191 (1990).
[4] O. Dutuit, M. C. Castex, J. Le Calvé, and M. Lavollée, J. Chem. Phys. **73**, 3107 (1980).
[5] W. Gornik, S. Kindt, E. Matthias, and D. Schmidt, J. Chem. Phys. **75**, 68 (1981).
[6] M. C. Castex, J. Chem. Phys. **74**, 759 (1981).
[7] W. Gornik, E. Matthias, and D. Schmidt, J. Phys. B **15**, 3413 (1982).
[8] D. Haaks and M. Swertz, Ann. Isr. Phys. Soc. **6**, 280 (1984).
[9] R. H. Lipson, P. E. LaRocque, and B. P. Stoicheff, J. Chem. Phys. **82**, 4470 (1985).
[10] P. M. Dehmer, S. T. Pratt, and J. L. Dehmer, J. Chem. Phys. **85**, 13 (1986).
[11] P. M. Dehmer, S. T. Pratt, and J. L. Dehmer, J. Phys. Chem. **91**, 2593 (1987).
[12] K. Tsukiyama, M. Tsukakoshi, and T. Kasuya, Chem. Phys. **127**, 393 (1988).
[13] R. H. Lipson, A. R. Hoy, and E. Chan, J. Chem. Phys. **90**, 4664 (1989).
[14] K. Tsukiyama and T. Kasuya, J. Mol. Spectrosc. **151**, 312 (1992).
[15] D. S. Green and S. C. Wallace, J. Chem. Phys. **100**, 6129 (1994).
[16] C. D. Pibel, K. Yamanouchi, and S. Tsuchiya, J. Chem. Phys. **100**, 6153 (1994).
[17] S. M. Koeckhoven, W. J. Buma, and C. A. de Lange, J. Chem. Phys. **99**, 5061 (1993).
[18] S. M. Koeckhoven, W. J. Buma, and C. A. de Lange, Phys. Rev. A **49**, 3322 (1994).
[19] *CRC Handbook of Chemistry and Physics*, 66th ed. edited by R. C. Weast (Chemical Rubber, Boca Raton, 1985–1986), p. E-259.
[20] G. Herzberg, *Molecular Spectra and Molecular Structure, I. Spectra of Diatomic Molecules* (Van Nostrand, Reinhold, 1950).
[21] D. E. Freeman, K. Yoshino, and Y. Tanaka, J. Chem. Phys. **61**, 4880 (1974).
[22] V. S. Vasan and R. J. Cross, J. Chem. Phys. **78**, 3869 (1983).
[23] G. Dahlquist, A. Björck, and N. Anderson, *Numerical Methods* (Prentice–Hall, New York, 1974).
[24] R. S. Mulliken, J. Chem. Phys. **52**, 5170 (1970).
[25] W. C. Ermler, Y. S. Lee, and K. S. Pitzer, J. Chem. Phys. **69**, 976 (1978).
[26] C. E. Moore, *Atomic Energy Levels* (U. S. GPO, Washington, D.C., 1971), No. C13.48:35, Vol. III, p. 113.
[27] M. Daskalopoulou, H. U. Böhmer, and S. D. Peyerimhoff, Z. Phys. D **15**, 161 (1990).
[28] R. G. Bray and R. M. Hochstrasser, Mol. Phys. **31**, 1199 (1976).
[29] C. Maïnos, Phys. Rev. A **33**, 3983 (1986).